



## Robust adaptive motion tracking of piezoelectric actuated stages using online neural-network-based sliding mode control

Jie Ling <sup>a,b,\*</sup>, Zhao Feng <sup>b</sup>, Dongdong Zheng <sup>c</sup>, Jun Yang <sup>c</sup>, Haoyong Yu <sup>c,\*</sup>, Xiaohui Xiao <sup>a</sup>

<sup>a</sup> College of Mechanical and Electrical Engineering, Nanjing University of Aeronautics and Astronautics, Nanjing 210016, China

<sup>b</sup> School of Power and Mechanical Engineering, Wuhan University, Wuhan 430072, China

<sup>c</sup> Department of Biomedical Engineering, National University of Singapore, Singapore 117608, Singapore



### ARTICLE INFO

#### Article history:

Received 12 April 2020

Received in revised form 4 August 2020

Accepted 22 August 2020

Available online 15 September 2020

#### Keywords:

Piezo-actuated stage  
Precision motion tracking  
Neural networks  
Robust adaptive control  
Sliding mode control  
Disturbance rejection

### ABSTRACT

Robust and precise motion tracking for micro-electro-mechanical systems in the presence of inherent nonlinearity and external disturbance is of great importance in many applications. Due to high sensitivity to environmental variations, the entire model or some parameters of the system tend to change unexpectedly. Existing offline nonlinearity models are computationally intensive and may be not suitable under system perturbations. In this work, for a class of piezoelectric actuated (PEA) system, a new online neural-network-based sliding mode control (OLNN-SMC) scheme is developed to obtain robust adaptive precision motions. The nonlinearity of the PEA system is identified online and compensated using singularity-free neural networks (NNs). To alleviate the residual NN approximation errors and meanwhile maintain robust stability under external disturbance, a feedback sliding-mode is synthesized into the control law. Considering unknown and varying disturbances, an adaptive mechanism is designed to achieve robust adaptive motion tracking. The controller is implemented and evaluated through experiments on a PEA platform. Results show that the proposed OLNN-SMC is superior to existing proportional-integral-derivative control with disturbance observer (PID+DOB) and adaptive sliding mode control (ASMC) in terms of sinusoidal tracking and disturbance rejection. In particular, the root-mean-square (RMS) errors for sinusoidal tracking at 0.1–10 Hz using the proposed OLNN-SMC are reduced by 83.5% compared with the cases using PID+DOB or ASMC.

© 2020 Elsevier Ltd. All rights reserved.

## 1. Introduction

Precision motion tracking has become increasingly important due to the rapid expansion of micro/nano-fabrication, microrobotics, microassembly, etc [1–4]. Due to the merits of rapid response, high accuracy and large driving force, piezoelectric actuators are widely adopted to provide precision motions in the above applications [5]. However, inherent nonlinearities of creep, hysteresis, and friction (in stick-slip stages [6]) of piezoelectric actuated (PEA) systems seriously influence the output motion precision [5,7]. In addition, unexpected disturbances may severely damage the stability of the whole system in operation [8]. Hence, control approaches to compensate nonlinearities and reject disturbance should be investigated to improve the motion accuracy of PEA systems.

\* Corresponding authors at: College of Mechanical and Electrical Engineering, Nanjing University of Aeronautics and Astronautics, Nanjing 210016, China (J. Ling).

E-mail addresses: [jamesling@whu.edu.cn](mailto:jamesling@whu.edu.cn) (J. Ling), [biehy@nus.edu.sg](mailto:biehy@nus.edu.sg) (H. Yu).

To achieve ideal cancellation of nonlinearities, appropriate mathematical models and control laws have been developed for PEA systems. Comprehensive surveys can be found in [5,9,10]. In terms of hysteresis cancellation, these works can be roughly classified into two categories as: i) feedforward control with hysteresis model and ii) feedback control without hysteresis model. Feedforward control laws are derived based on inverse models to compensate the nonlinearities [7,11–13]. Besides, inversion-free predictive controllers based on neural networks have been proposed to relieve computation burden for inverse models [14,15]. Feedforward controllers are effective and efficient provided that offline models are available and accurate [9–15], however, environmental perturbations (i.e., temperature or load change) will lead to system parameter variation. In these cases, offline models identified or trained in advance will not fit the actual systems. As a result, feedforward controllers based on these models will not perform as expected.

For feedback control, tracking performance can be guaranteed by treating the nonlinearities as unmodeled dynamics or unknown disturbances [5]. Robust  $H_\infty$  controllers were implemented to eliminate the undesirable nonlinear effects of PEA systems in [16,17]. To enhance the stability under unknown hysteretic disturbances, sliding mode controllers (SMCs) were widely studied [18–21]. A sliding mode observer with a proportional-integral-derivative-based switching function is used for tracking control of PEA systems in [18]. By estimating the hysteresis effects using a perturbation estimation technique, a sliding mode robust controller was proposed in [19]. However, to satisfy the reaching conditions in SMCs, model perturbation range needs to be known clearly. To overcome this shortcoming in SMCs, adaptive laws are usually introduced for parameter adaption to synthesize robust adaptive controllers [1,20,21]. An enhanced adaptive sliding mode control was developed for PEA systems to obtain both chattering-free transient performance and final tracking precision in [1]. Another challenge in feedback loops is to maintain stability in the presence of external disturbances. For this, an adaptive disturbance observer-based SMC was recently proposed for a PEA surgical device in [8]. It can be found from the above works that feedback control has the ability of dealing with system uncertainties and the robustness against parameter variations to some extent. However, when model uncertainties coupled with strong nonlinear behaviors and external disturbances in PEA systems, control gains can not always be chosen sufficiently large under feedback control alone [5]. With respect to this circumstances, tracking errors will be increased, and the stability of the closed-loop systems may not be guaranteed.

Alternatively, other feedback controllers with intelligent techniques have also been attempted to deal with precision motion tracking of PEA systems. Neural-network-based adaptive controllers were tested for compensating hysteresis induced by friction in [22,23]. However, the inherent hysteresis of piezoceramics and external disturbance were not considered. A novel neural networks based composite scheme had been proved effective to control the nonlinearities of friction and hysteresis existed in a PEA surgical device [24]. The control law in [24] consisted of neural networks based sliding mode component and extended state observer (ESO) based component, which combined both the advantages of the feedforward and feedback control. It should be pointed out that a main drawback of the composite scheme was the intensive computation and limited bandwidth in real-time implementation resulted from the ESO component [25]. In addition, considering the possible parameter variation in PEA systems' applications, singularity problem may occur from the denominator of the control law [26]. Recently, it has been reported in [27] that a novel online neural-network-based scheme has the potential to deal with identification and control of nonlinear systems without the singularity problem. However, it is uncertain whether the scheme is applicable to a PEA system with inherent nonlinearities and external disturbances simultaneously.

To this end, a new online neural-network-based sliding mode control (OLNN-SMC) scheme is proposed in this paper to design a composite controller without the singularity issue and computationally intensive disturbance observers. Firstly, a singularity-free approach is adopted to make online identification and compensation of nonlinearities (hysteresis and friction) of a PEA system. As for the residual matching errors, unmodeled uncertainties, and external disturbances, a sliding mode controller is then constructed to guarantee tracking errors' convergence. Then, the feedback control gain is designed adaptive according to a lumped disturbance such that a robust adaptive motion tracking can be achieved. Thus, the proposed composite control law includes two parts: i) a feedforward component for cancelling of nonlinearities based on singularity-free neural networks; ii) a feedback component for maintaining robust stability under disturbances using an adaptive sliding mode. The stability of the proposed OLNN-SMC law is demonstrated in theory, and its effectiveness is verified through comprehensive experimental studies on a PEA motion platform developed in [6].

The main contribution of this work is that it not only provides a new online identification and control scheme for PEA systems, but also induces a rigorous theoretical support for precision motion tracking of the scheme under unknown disturbances. Unlike existing neural-network-based schemes in [22,24,28], a singularity-free approach [27] is adopted to smooth the online identification process. Moreover, no additional disturbance observer (DOB) as in [24] is needed for disturbance rejection to relieve computation burden for controller hardware in practical applications. The proposed OLNN-SMC scheme is attractive for practical uses with the characteristics as:

- 1) Nonlinearity model free for controller synthesis;
- 2) Singularity free during identification and control process;
- 3) Robust stability to external disturbances without using any ESO or DOB;
- 4) Adaptive ability to unknown disturbances and system parameter variations.

The reminder of this paper is arranged as follows. The system modeling and control problem are described in Section 2. The neural-network-based online identification for the PEA systems is discussed in Section 3. Then, the new OLNN-SMC

scheme and the control gain design are presented in Section 4. Controller implementation is presented in Section 5. Experimental studies and comparisons are made in Section 6. Some concluding remarks are drawn in Section 7.

## 2. Problem formulation

**Notations:** In the following sections,  $\mathbb{R}$ ,  $\mathbb{R}^+$  and  $\mathbb{R}^n$  represent the real number space, positive real number space and real  $n$ -vector space, respectively,  $\Omega_c := \{\mathbf{x} \mid \|\mathbf{x}\| \leq c\}$  denotes the ball of radius  $c$ ,  $\|\mathbf{x}\|$  is the Euclidean norm of  $\mathbf{x}$ .

### 2.1. System description

In general, the model of a PEA system can be divided into a nonlinear operator cascaded with linear dynamics [5,10,11], which is called a Hammerstein architecture as shown in Fig. 1. Nonlinearities of creep and hysteresis are hard to be characterized and modeled when associated with frictions in some PEA systems like stick-slip motion stages in [6] or surgical devices in [24].

We consider a general PEA system in Fig. 1 represented by the following dynamics as [1,24]:

$$m\ddot{x}(t) + b\dot{x}(t) + h(t) = au(t) + d(t), \quad (1)$$

where  $t$  stands for the time variable,  $x \in \mathbb{R}$  and  $u \in \mathbb{R}$  are the output displacement and input driving voltage of the PEA system,  $a \in \mathbb{R}$  is denoted as an electromechanical ratio from  $u$  to  $x$ ,  $\dot{x} \in \mathbb{R}$  and  $\ddot{x} \in \mathbb{R}$  are the velocity and acceleration,  $m \in \mathbb{R}$ ,  $b \in \mathbb{R}$ ,  $k \in \mathbb{R}$  are the effective mass, damping and stiffness coefficients, respectively. Besides,  $h \in \mathbb{R}$  denotes the nonlinear effects including the creep, hysteresis, and friction,  $d \in \mathbb{R}$  represents the lumped external disturbances. It is reasonable to assume that the terms  $h$  and  $d$  are bounded. Thus, the following assumption is imposed.

**Assumption 1.** All the states are bounded for a physical system, and  $h(t)$  and  $d(t)$  are bounded such that

$$|h(t)| \leq \bar{h}, |d(t)| \leq \bar{d}, \quad (2)$$

where the constants  $\bar{h} \in \mathbb{R}^+$ ,  $\bar{d} \in \mathbb{R}^+$ .

To facilitate the online neural networks, the system in (1) is rewritten into the form,

$$\dot{x} = f(\mathbf{x}) + b_m u + d_m \quad (3)$$

where the time variable  $t$  is omitted for brevity,  $\mathbf{x} = [x, \dot{x}]^T \in \mathbb{R}^2$ , and  $f(\mathbf{x}) : \mathbb{R}^2 \mapsto \mathbb{R}$  is the unknown continuous function which contains both the linear and nonlinear components, i.e.,  $f(\mathbf{x}) = (-bx - kx - h)/m$ ,  $d_m = d/m$  and  $b_m = a/m$  are the scaled coefficient or variable in (1). It can be inferred from Assumption 1 that both  $f(\mathbf{x})$  and  $d_m$  are also bounded.

### 2.2. Control objective

According to the preliminaries, the control problem can then be formulated here. Given a desired position trajectory  $x_d$ , the control objective is to obtain precision motion tracking of  $x_d$  for the system in (1) without any offline model or any disturbance observer. In order to improve the robustness and adaptivity in the presence of dynamic uncertainties  $f(\mathbf{x})$  and unknown disturbances  $d_m$ , a robust adaptive OLNN-SMC scheme is proposed in the following Sections 3 and 4.

## 3. Online system identification

### 3.1. Online neural networks

#### 3.1.1. Conventional NN design

For an unknown nonlinear system in (3), a conventional NN approach [22–24,28], is to adjust weights and finally obtain proper NNs which can estimate  $f(\mathbf{x})$  and  $b_m$  with minimized errors as,

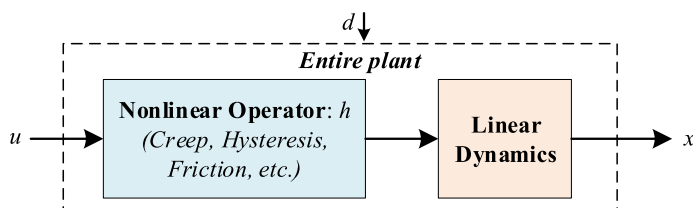


**Fig. 1.** The Hammerstein architecture of a piezoelectric actuated system consisting of a nonlinear model cascaded with linear dynamics.

$$\min_{\hat{W}_0} e_x := \min_{\hat{W}_0} (x - \hat{x}), \quad (4)$$

with

$$\begin{cases} \ddot{x} = W^* \Phi(x) + b_m u + \zeta_x \\ \ddot{\hat{x}} = \hat{W} \Phi(x) + \hat{b}_m u + L(\dot{x} - \dot{\hat{x}}), \end{cases} \quad (5)$$

where  $\Phi(x)$  is the NN basis vector designed by the user,  $W^*$  is the ideal NN weight vector which can minimize the bounded approximation error  $\zeta_x$ ,  $\hat{x}$ ,  $\hat{W}$  and  $\hat{b}_m$  are the estimations of  $x$ ,  $W^*$  and  $b_m$ , respectively,  $L$  is the observer gain selected by the designer,  $\hat{W}_0 := [\hat{W}, \hat{b}_m]$  is represented as an augmented weight vector.

Through the identification process of (4), a set of proper weights and regressor can be obtained directly, which can further be used to design feedback or feedforward controller for some certain purposes. However, it should be noted that a projection mechanism is always needed to avoid the singularity problem as  $1/(\hat{b}_m)$  is always necessary in a feedback adaptive controller design [28]. To avoid this problem, we apply the singularity-free NNs for the online identification of a PEA system as follows.

### 3.1.2. Proposed online NN design

In order to develop the online NN, a reformulation should be conducted for the system in (3). Divide both the two sides of the dynamics by  $b_m$ , an equivalent form of the system can be obtained as,

$$b_m^{-1} \ddot{x} = b_m^{-1} f(x) + u + b_m^{-1} d_m. \quad (6)$$

According to Lemma 4 concerning spatially localized approximation in [29], a set of proper NNs can always be found to represent system dynamics in (6) as,

$$c^* \ddot{x} = W^* \Phi(x) + u + \zeta_x, \quad (7)$$

where  $\zeta_x \in \mathbb{R}$  is a residual error which contains bounded NN approximation error and bounded external disturbance,  $\Phi(x) = [\phi_1(x), \phi_2(x), \dots, \phi_n(x)]^T \in \mathbb{R}^n$  with  $n \in \mathbb{R}^+$  is the NN basis vector designed by the user,  $c^*$  is the ideal value of  $b_m^{-1}$ ,  $W^* := [\omega_1^*, \omega_2^*, \dots, \omega_n^*] \in \mathbb{R}^n$  is the ideal NN weights which minimize  $\zeta_x$ .

**Remark 1.** It should be noted that in the stage of online system identification, external disturbance is bounded for a physical system according to Assumption 1. In this stage, only system dynamics are approximated by NNs. In the latter controller design in Section IV, residual error due to external disturbance will be reconsidered to synthesis the adaptive sliding mode controller.

It can be seen from (7) that derivatives of system states are needed to update NN weights if conventional design (e.g., [22–24,28]) of NNs are applied. However, for practical applications, high-frequency noises are always included in the measured signals, which will lead to increased noise density after the differentiation operation. For this, identification accuracy will be reduced, and the stability of the training scheme will be threatened. In the proposed online NN design, by applying a filtering operation, noise density can be weakened as a result of an introduced low pass filter. Thus, the proposed online NN scheme is more robust to measurement noises compared with conventional NNs.

Define a stable low-pass filter  $Q = 1/(\gamma s + 1)$ , where  $\gamma$  is the time constant of the filter. Filter both the two sides of (7) using  $Q$ , the system can be reorganized as

$$u_f = -W^* \Phi_f(x) + c^* \ddot{x}_f - \zeta_{x_f} := \Theta^* \Psi + \Delta_x, \quad (8)$$

where  $(\cdot)_f$  denotes the filtered signal of  $(\cdot)$  with  $(\cdot)_f(0) = 0$ , the argumented vectors  $\Theta^* = [c^*, -W^*] \in \mathbb{R}^{n+1}$ ,  $\Psi = [\ddot{x}_f; \Phi_f(x)] \in \mathbb{R}^{n+1}$ ,  $\Delta_x = -\zeta_{x_f} + c^* \delta_x$ .

**Remark 2.** To obtain  $\ddot{x}_f$  in (8), one can filter the observed state  $\dot{x}$  instead of  $\ddot{x}$  and conduct the following operation to attenuate the effects of noise [27,30],

$$\dot{x}_f = \frac{\dot{x}}{\gamma s + 1} \iff \ddot{x}_f = \frac{\dot{x} - \dot{x}_f}{\gamma}, \quad (9)$$

where  $\gamma \in \mathbb{R}^+$  is selected by the designer according to the operation bandwidth of the system.

### 3.1.3. Update law design for weights of NNs

Define two auxiliary regressors  $M(t) \in \mathbb{R}^{(n+1) \times (n+1)}$  and  $N(t) \in \mathbb{R}^{(n+1) \times 1}$  in the NNs as,

$$M(0) = \mathbf{0} \in \mathbb{R}^{(n+1) \times (n+1)}, \quad \dot{M} = -\mu M + \frac{\mu \Psi \Psi^T}{v + \Psi^T \Psi}, \quad (10)$$

$$N(0) = \mathbf{0} \in \mathbb{R}^{(n+1) \times 1}, \quad \dot{N} = -\mu N + \frac{\mu \Psi u_f}{v + \Psi^T \Psi}, \quad (11)$$

where  $\mu \in \mathbb{R}^+$ ,  $v \in \mathbb{R}^+$  are positive user-defined parameters.

$M$  and  $N$  can be viewed as the filtered results of  $\Psi \Psi^T$  and  $\Psi u_f$ , and  $\mu$  is the filter parameter which determines the bandwidth. Therefore, a larger  $\mu$  means a higher filter bandwidth, and faster convergence of NN weight can be achieved. However, the updating of the NN will also be more sensible to measurement noise or external disturbance. On the contrary, if  $\mu$  is small, the convergence of the NN will also be slow. Nevertheless, the NN training will be more robust to measurement noise or external disturbance. Usually setting  $\mu = 0\text{--}1$  can result in a good result.  $v + \Psi^T \Psi$  is used for normalization to avoid dramatic change of the NN weights when  $\Psi$  or  $u_f$  is large.  $v$  is a small parameter (usually between 0.001–1, the choice of  $v$  is not crucial to the training result of the NN) to avoid the potential singularity problem when  $\Psi^T \Psi = 0$ .

Solve the equations of (10) and substitute (9) into (11), following results can be obtained as

$$M(t) = \int_0^t e^{-\mu(t-\tau)} \frac{\mu \Psi \Psi^T}{v + \Psi^T \Psi} d\tau, \quad (12)$$

$$\begin{aligned} N(t) &= \int_0^t e^{-\mu(t-\tau)} \frac{\mu \Psi (\Psi^T \Theta^* + \Delta_{x_f})}{v + \Psi^T \Psi} d\tau \\ &= M(t) \Theta^{*T} + \bar{\Delta}_x, \end{aligned} \quad (13)$$

with

$$\bar{\Delta}_x = \int_0^t e^{-\mu(t-\tau)} \frac{\mu \Psi \Delta_{x_f}}{v + \Psi^T \Psi} d\tau. \quad (14)$$

It can be inferred from (9) that  $\Delta_{x_f}$  is bounded. For this,  $\bar{\Delta}_x$  is also bounded in (13). Define an auxiliary weight error vector as,

$$\begin{aligned} \Xi &= N - M \hat{\Theta}^T \\ &= M \tilde{\Theta}^T - \bar{\Delta}_x, \end{aligned} \quad (15)$$

with

$$\tilde{\Theta} = \Theta^* - \hat{\Theta}, \quad (16)$$

where  $\hat{\Theta} := [\hat{c}, -\hat{W}]$  with  $\hat{c}$  and  $\hat{W}$  denoting the estimations of  $c^*$  and  $W^*$  in (8),  $\tilde{\Theta}$  stands for the weight estimation error vector between  $\Theta^*$  and  $\hat{\Theta}$ . It can be clearly seen that estimation errors of the NN weights are included in  $\Xi$ , therefore the learning algorithm to update the NN weights is proposed as

$$\dot{\tilde{\Theta}} = \rho \Xi, \quad (17)$$

where  $\rho \in \mathbb{R}^+$  is an user-defined positive parameter. It is suggested to set it as a small value in the beginning, and then tuned to be larger enough gradually in the experiments according to tradeoff between convergence rate and chattering.

The following **Theorem 1** can be established with respect to the convergence of the proposed online NN for approximation of the nonlinear PEA system (3).

**Theorem 1.** Consider the filtered online neural network in (8). If  $\Psi$  is persistently excited, then by using learning algorithm provided in (17), the weight estimation error vector  $\tilde{\Theta}$  is ultimately uniformly bounded (UUB) and exponentially converges to a compact set around  $\mathbf{0}$ .

**Proof.** Choose the Lyapunov function candidate as,

$$V_1 = \frac{1}{2} \tilde{\Theta} \tilde{\Theta}^T. \quad (18)$$

Applying (17), the differentiation of  $V_1$  can be expressed as,

$$\begin{aligned} \dot{V}_1 &= \tilde{\Theta} \dot{\tilde{\Theta}}^T \\ &= -\rho \tilde{\Theta} M \tilde{\Theta}^T + \rho \tilde{\Theta} \bar{\Delta}_x. \end{aligned} \quad (19)$$

As  $\Psi$  is persistently excited, there exists  $T > 0$ ,  $\alpha > 0$  such that  $\forall t > 0$  ([27,29]),

$$\int_t^{t+T} \Psi \Psi^T dr \geq \alpha I. \quad (20)$$

Herein, it can be inferred from (12) and (20) that,

$$\begin{aligned} M(t) &> e^{-\mu T} \int_{t-T}^t \frac{\mu \Psi \Psi^T}{v + \Psi^T \Psi} d\tau \\ &> \beta I, \end{aligned} \quad (21)$$

where  $\beta = e^{-\mu T} \varrho \alpha$ , and  $\varrho$  is introduced as the lower bound of  $\mu / (v + \Psi^T \Psi)$ .

Sequently,  $\dot{V}_1$  can be further derived as,

$$\begin{aligned} \dot{V}_1 &< -\rho \beta \cdot \tilde{\Theta} \tilde{\Theta}^T + \rho \cdot \tilde{\Theta} \bar{\Delta}_x \\ &\leq -\rho \beta \cdot \tilde{\Theta} \tilde{\Theta}^T + \frac{\rho \beta}{2} \tilde{\Theta} \tilde{\Theta}^T + \frac{\rho}{2\beta} \bar{\Delta}_x^T \bar{\Delta}_x \\ &\leq -\frac{\rho \beta}{2} \tilde{\Theta} \tilde{\Theta}^T + \frac{\rho}{2\beta} \bar{\Delta}_x^T \bar{\Delta}_x \\ &= -\eta V_1 + \zeta \end{aligned} \quad (22)$$

where  $\eta := \rho \beta$ ,  $\zeta := (\rho / 2\beta) \bar{\Delta}_x^T \bar{\Delta}_x$ . On the basis of the well-known Lyapunov stability theorem [31], it is inferred that  $V_1$  and the weight estimation error vector  $\tilde{\Theta}$  are UUB, which also indicates that  $\hat{W}_1$  and  $\hat{W}_2$  are bounded.

In addition, by solving (22), one can obtain

$$\begin{aligned} V_1(t) &= \frac{1}{2} \tilde{\Theta}(t) \tilde{\Theta}^T(t) \\ &\leq e^{-\eta t} V_1(0) + \frac{\zeta}{\eta}, \end{aligned} \quad (23)$$

which implies that  $V_1(t)$  converges to a small residual approximation error exponentially, i.e.,  $\tilde{\Theta}$  converges exponentially to a small residual neighborhood of  $\mathbf{0}$  as,

$$\Omega = \left\{ \tilde{\Theta} \mid \tilde{\Theta} \tilde{\Theta}^T \leq \frac{2\zeta}{\eta} \right\}. \quad (24)$$

Thus, [Theorem 1](#) is proved.

**Remark 3.** Compared with traditional neural networks in [30,32–34], there are mainly two advantages of the adopted online neural networks over traditional neural networks:

- 1) Singularity-free property during the online identification process. For a class of nonlinear systems in (3) with unknown control gain  $b_m$ , a traditional strategy is to obtain an approximation  $\hat{b}_m$  of  $b_m$  online using an NN method, and then a feedforward or feedback controller can be designed. However, because of the common usage of  $\hat{b}_m^{-1}$  in calculating the controller, a computational singularity problem may occur in the controller implementation if  $\hat{b}_m^{-1}$  tends to be quite small or even to zero in the updating process. To avoid the singularity problem, a singularity-free online NN method is applied to approximate  $\hat{b}_m^{-1}$  directly instead of the usage of a deadzone or projection mechanism;
- 2) Usage of lower-order system states. In conventional design of NNs, derivatives of system states are needed to update NN weights. In practical application, high-frequency noises are always included in the measured signals, which will lead to increased noise density after the differentiation operation. For this, identification accuracy will be reduced, and the stability of the training scheme will be threatened. In the singularity-free NN design, by applying the filtering operations as presented in (9), derivatives of system states are evitable. Thus, lower-order system states are required in the adopted online NN. Moreover, the noise density can be weakened as a result of the introduced low pass filter. Thus, the online NN scheme is more robust to measurement noises compared with conventional NNs.

#### 4. Proposed neural-network-based sliding mode control

Recall the PEA system in (7) and take the lumped external disturbance into consideration as in (1), the system can then be represented as,

$$c^* \ddot{x} = W^* \Phi(x) + u + c^* d_m + \zeta_x, \quad (25)$$

where,  $c^* d_m$  stands for the external disturbance,  $\zeta_x$  is the approximation error between ideal NNs and actual dynamics. It can be found from [Assumption 1](#) and [Theorem 1](#) that, the two items are bounded so than the system can be rewritten as,

$$c^* \ddot{x} = W^* \Phi(x) + u + d_l, \quad (26)$$

where the lumped disturbance  $d_l = c^* d_m + \zeta_x$  with  $|d_l| \leq \bar{d}_l \in \mathbb{R}^+$ .

##### 4.1. Controller design

The goal of the control scheme is to minimize the position tracking error in the presence of the lumped disturbance  $d_l$  as

$$e = x - x_d, \quad (27)$$

where  $x_d$  is the desired position trajectory.

To achieve convergence of the desired trajectory and minimize steady-state error, a proportional-derivative type sliding function is adopted in this paper, which is defined as

$$\sigma = \lambda e + \dot{e}, \quad (28)$$

where  $\lambda \in \mathbb{R}^+$  is a constant defined by the user. As (28) is continuous and differentiable, the deviation of  $\sigma$  is derived as,

$$\begin{aligned} c^* \dot{\sigma} &= c^* \lambda \dot{e} + c^* \ddot{e} \\ &= c^* \lambda \dot{e} + (W^* \Phi + u + d_l) - c^* \ddot{x}_d. \end{aligned} \quad (29)$$

Making  $\dot{\sigma} = 0$  and  $d_l = 0$ , and adopting the online NN regressors for the unknown system, an equivalent control input can be calculated as

$$u_{eq} = \hat{c}(-\lambda \dot{e} + \ddot{x}_d) - \hat{W} \Phi. \quad (30)$$

To compensate the lumped disturbance  $d_l$  as well as the residual error between trained NNs and ideal NNs, a switching control input is designed as

$$u_{sw} = -k_s \cdot \text{sign}(\sigma) - k_\sigma \sigma, \quad (31)$$

where  $k_s \in \mathbb{R}^+$  is the switch gain to be tuned by the user,  $k_\sigma \in \mathbb{R}^+$  is an user-defined parameter.

To this end, the following theorem is proposed for the robust motion tracking of the PEA system.

**Theorem 2.** For a PEA system in (25), the sliding function  $\sigma$  and the motion tracking error  $e$  will converge to a compact set around  $\mathbf{0}$  if the following composite control law is used

$$\begin{aligned} u &= u_{eq} + u_{sw} \\ &= \hat{c}(-\lambda \dot{e} + \ddot{x}_d) - \hat{W} \Phi - k_s \text{sign}(\sigma) - k_\sigma \sigma, \end{aligned} \quad (32)$$

where the gains should satisfy that  $k_s \geq \bar{d}_l, k_\sigma \in \mathbb{R}^+$ .

**Proof.** To analyze the stability of the composite control law, a Lyapunov function candidate is selected as,

$$V_2 = V_1 + \frac{c^*}{2} \sigma^2. \quad (33)$$

Then,  $\dot{V}_2$  can be obtained using (29) and (32) as,

$$\begin{aligned} \dot{V}_2 &= \dot{V}_1 + \sigma \cdot c^* \dot{\sigma} \\ &= \dot{V}_1 + \sigma(c^* \lambda \dot{e} + W^* \Phi + u + d_l - c^* \ddot{x}_d) \\ &= \dot{V}_1 + \sigma \cdot (d_l + \tilde{\Theta} \Upsilon - k_s \text{sign}(\sigma)) - k_\sigma \sigma^2, \end{aligned} \quad (34)$$

where  $\Upsilon = [\lambda \dot{e} - \ddot{x}_d; -\Phi]$ . Note that  $\Upsilon$  is bounded for a PEA system for that all the states are bounded, i. e.,  $\|\Upsilon\| \leq \bar{v} \in \mathbb{R}^+$ . According to Young's inequality,  $\sigma \tilde{\Theta} \Upsilon \leq \frac{v}{2} \sigma^2 + \frac{v}{2} \tilde{\Theta} \tilde{\Theta}^T = \frac{v}{2} \sigma^2 + \bar{v} V_1$ . Herein, combining with (22),  $\dot{V}_2$  can be rewritten as,

$$\begin{aligned} \dot{V}_2 &\leq -(\eta - \bar{v}) V_1 - (k_\sigma - \bar{v}/2) \sigma^2 + \zeta + \sigma(d_l - k_s \text{sign}(\sigma)) \\ &\leq -\eta_2 V_2 + \zeta + \sigma(d_l - k_s \text{sign}(\sigma)), \end{aligned} \quad (35)$$

where  $\eta_2 = \min\{\eta - \bar{v}, \frac{2k_\sigma - \bar{v}}{c^*}\}$ . Therefore, tune  $k_s$  such that  $k_s \geq \bar{d}_l$ , then  $\dot{V}_2 \leq -\eta_2 V_2 + \zeta$ . By solving this inequation, one can obtain that,

$$V_2(t) \leq e^{-\eta_2 t} V_2(0) + \frac{\zeta}{\eta_2}, \quad (36)$$

which implies that  $V_2(t)$  converges to a small residual approximation error exponentially, and the NN weights approximation error and the motion tracking error will converge exponentially to a compact set of  $\mathbf{0}$ . **Theorem 2** is proved.

#### 4.2. Parameter adaptation

It can be seen from **Theorem 2** that the switch gain  $k_s$  should be specified in advance based on the upper bound of the lumped disturbance  $\bar{d}_l$ . However, as stated in (26), this disturbance covers unmatched dynamics resulted from NN approximation and external disturbance, which is complicated so that it is hard to estimate the upper bound properly. To handle this issue,  $k_s$  is always set big enough to maintain the robustness to disturbance. However, this conservative method may result in chattering vibration and deteriorating the tracking performance subsequently.

In this work, we consider an adaptive technology to be utilized for  $k_s$  to alleviate the problem. An auxiliary variable to represent the estimated error of  $k_s$  as  $\tilde{k}_s = \hat{k}_s - k_s$ , where  $\hat{k}_s$  is the estimated gain of  $k_s$ . The following Theorem can be given for the adaptive design.

**Theorem 3.** For a PEA system in (25), the sliding function  $\sigma$  and the motion tracking error  $e$  will converge to a compact set around  $\mathbf{0}$  if the following adaptive control law is applied

$$u = \hat{c} \cdot (-\lambda \dot{e} + \ddot{x}_d) - \hat{W}\Phi - \tilde{k}_s \text{sign}(\sigma) - k_\sigma \sigma, \quad (37)$$

with the adaptive law given as

$$\dot{\tilde{k}}_s = \alpha(|\sigma| + k_\alpha \sigma), \quad (38)$$

where  $\alpha \in \mathbb{R}^+$  is the adaptive gain,  $k_\sigma, k_\alpha \in \mathbb{R}^+$  are user-defined parameters.

**Proof.** A Lyapunov function candidate is chosen as

$$V_3 = V_2 + \frac{1}{2\alpha} \tilde{k}_s^2, \quad (39)$$

which will lead to

$$\dot{V}_3 = \dot{V}_2 + \alpha^{-1} \tilde{k}_s \dot{\tilde{k}}_s. \quad (40)$$

Substitute (29) and (37) into (40), one can obtain

$$\dot{V}_3 \leq -\eta_2 V_2 + \zeta + \sigma(d_l - \hat{k}_s \text{sign}(\sigma)) + \tilde{k}_s |\sigma| + \tilde{k}_s k_\alpha \sigma. \quad (41)$$

Note that  $|\sigma| = \sigma \text{sign}(\sigma)$ , thus  $\sigma(d_l - \hat{k}_s \text{sign}(\sigma)) + \tilde{k}_s |\sigma| = \sigma(d_l - k_s \text{sign}(\sigma))$ . Using Young's inequality,  $\tilde{k}_s k_\alpha \sigma \leq \frac{k_\alpha}{2} (\tilde{k}_s^2 + \sigma^2)$ , then  $V_3$  can be further derived as

$$\dot{V}_3 \leq -\eta_3 V_3 + \zeta + \sigma(d_l - k_s \text{sign}(\sigma)), \quad (42)$$

where  $\eta_3 = \min\{\eta_2, \eta_2 - \frac{k_\alpha}{c^*}, -\alpha k_\alpha\}$ . As  $k_s \geq \bar{d}_l$ , it can be obtained that  $\dot{V}_3 \leq -\eta_3 V_3 + \zeta$ . This implies that  $V_3(t)$  converges to a small residual approximation error exponentially. Thus, Theorem 3 is proved.

Due to inevitable noise existing in the experiments, undesired drifts may occur in the adaption process. To avoid this, a dead-zone technique can be utilized to switch off the adaptive law when the tracking error is decreased below an acceptable threshold [1]. Herein, the adaptive law is modified as

$$\dot{\tilde{k}}_s = \begin{cases} 0, & \text{if } |e| \leq \delta \\ \alpha(|\sigma| + k_\alpha \sigma), & \text{if } |e| > \delta, \end{cases} \quad (43)$$

where  $\delta \in \mathbb{R}^+$  is a defined threshold for tracking error. This can be treated as an error boundary which can be approached by the proposed control scheme.

To this end, the composite control law is derived as

$$u = \underbrace{-\hat{W}\Phi}_{u_{nn}} + \underbrace{\hat{c} \cdot (-\lambda \dot{e} + \ddot{x}_d) - \tilde{k}_s \text{sign}(\sigma) - k_\sigma \sigma}_{u_{smc}}, \quad (44)$$

where  $u_{nn}$  and  $u_{smc}$  are respectively the control signals generated by online neural networks based nonlinearity compensator and the adaptive sliding mode controller, the weights  $\hat{W}$  are updated using (17), the controller gain is adaptive using (43). The overall control scheme is shown in Fig. 2.

**Remark 4.** The control schemes in [22,23] applied neural network-based adaptive techniques to compensate hysteresis induced by friction. However, the inherent hysteresis of piezoceramics and external disturbance were not considered. Also, the singularity problem in the online NN identification is not considered. In this scheme, the nonlinearity is compensated by singularity-free neural networks, which is superior to the NNs in [22,23] to handle with the singularity issue during online identification process. In addition, there are no additional disturbance observers in the proposed scheme for disturbance rejection, thus the computation burden is relieved to some extent for the implementation of controller hardware compared with [24].

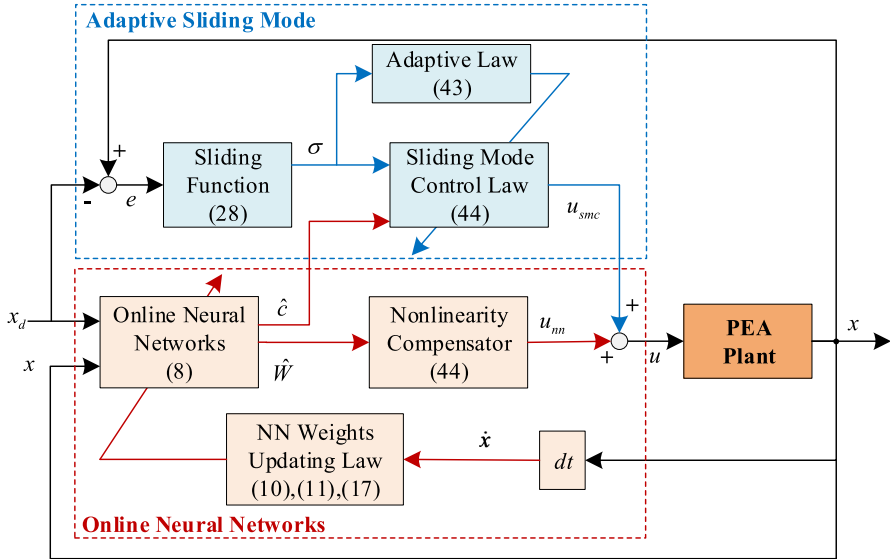


**Fig. 2.** The overall control scheme of the proposed OLNN-SMC for a PEA system.

## 5. Controller implementation

The experimental system adopted in this paper is depicted in Fig. 3. A custom-designed PEA stage in [6] is utilized in this work for the verification of the proposed control scheme.

The control input voltage with a range of 0–10 V is produced by 16-bit digital to analog interfaces (model: DS2102 D/A Board, from dSPACE Co., Ltd.) of the data output module in real-time controller (model: DS1007 PPC Processor Board, from dSPACE Co., Ltd.). A piezo amplifier module (model: ENP-151U, from ECHO ELECTRONICS Co., Ltd.) with a fixed gain amplifies the input voltage and generates excitation voltage. The output displacement is read by a laser sensor (model: LK-H052, from KEYENCE Co., Ltd.), and is subsequently passed to the data input module in a dSPACE control system with 16-bit analog to digital interfaces (model: DS2002 A/D Board, from dSPACE Co., Ltd.).

The controller is designed in MATLAB®/Simulink block diagram on the host computer (running on Windows 7 and an Intel Core i7-4770 CPU), where the Solver is chosen as fixed-step ode 4 with a step size being 0.2 ms, and then downloaded and executed on a target dSPACE in the real-time software environment of dSPACE ControlDesk.

### 5.1. Controller set

To evaluate the performance of the proposed OLNN-SMC scheme, another two existing schemes are also implemented in this paper to make fair comparisons. The controller set is arranged as: 1) Feedback Proportional-integral-derivative control with a disturbance observer (PID+DOB) [35]; 2) Adaptive sliding mode control (ASMC) [8]; 3) The proposed OLNN-SMC in this paper.

#### 5.1.1. PID+DOB

For this scheme, external disturbance is observed and compensated in advance through a well-defined DOB [35]. The transfer function  $T_{d,x}$  from disturbance  $d$  to output  $x$  is derived as,

$$T_{d,x}(s) = \frac{G(s)(1 - Q(s))}{1 + C(s)G(s) + Q(s)\left(1 - G(s)G^{-1}(s)\right)}, \quad (45)$$

where  $s$  is the frequency variable,  $G$ ,  $Q$ ,  $C$  are the nominal model, low-pass filter and feedback controller, respectively. It can be seen that disturbance within the filter bandwidth can be compensated through the well-defined DOB. The control law of a PID+DOB scheme can be given as,

$$u_1 = k_p e + k_i \int edt + k_d \dot{e} - \hat{d}, \quad (46)$$

where  $k_p$ ,  $k_i$ ,  $k_d$  are the controller gains,  $e$  is the tracking error,  $\hat{d}$  is the observed disturbance which is related to the identified nominal model  $G$  and the bandwidth of a low-pass filter  $Q$ . According to the nominal system, the gains are tuned using

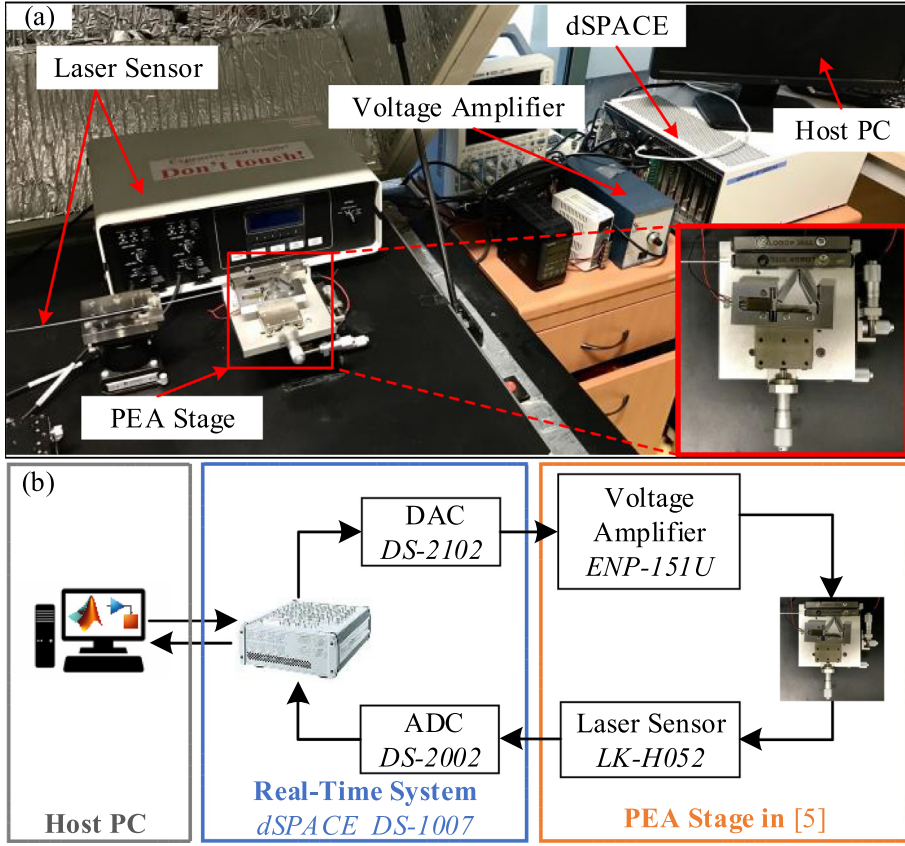


**Fig. 3.** Experimental setup of a piezo-actuated stage developed in [6]: (a) experimental system; (b) block diagram of signal flow.

the ‘*pidtune*’ command in MATLAB for the feedback PID, and the bandwidth of the low-pass filter is set as 100 Hz which is large enough to cover the operating bandwidth.

### 5.1.2. ASMC

For the system in (1), an ASMC control law proposed in [8] is given as

$$u_2 = m_n(\ddot{x}_d + K_v \dot{e}_r + K_p e_r) + b_n \dot{x}_n + k_n x_n + \frac{1}{\hat{a}} [\hat{m} \ddot{x}_d - \hat{m} \lambda_2 \dot{e}_p + \hat{b} \dot{x} + \hat{k} x - e_p - K_c \sigma_2 - K_s \text{sat}(\frac{\sigma_2}{\epsilon})], \quad (47)$$

where,  $m_n$ ,  $b_n$  and  $k_n$  are the parameters of a pre-defined nominal model  $G_n$ ,  $e_r = x_d - x_n$  is denoted as the errors between the desired output  $x_d$  and the nominal output  $x_n$  of  $G_n$ ,  $e_p = x - x_n$  is the errors between the actual output  $x$  and  $x_n$ , the sliding manifold is defined as  $\sigma_2 = \dot{e}_p + \lambda_2 e_p$  with  $\lambda_2 \in \mathbb{R}^+$ .  $K_p$  and  $K_v$  are the feedback position and velocity gains, and they are chosen to eliminate servo velocity error and servo position error between the desired and nominal trajectory. Normally, they can be primarily tuned according to the identified nominal model  $G$  and the pre-defined ideal nominal model  $G_n$ .  $\hat{m}$ ,  $\hat{b}$ ,  $\hat{k}$  and  $\hat{a}$  are the estimated values of the system in (1).  $K_c$ ,  $K_s$  are the parameters to be tuned for convergence, which are always selected as a small value in the beginning and then tuned to be larger enough gradually in the experiments according to the convergence rate and chattering.  $\epsilon \in \mathbb{R}^+$  is a small constant, which denotes the width of the boundary layer. This is used to stop the adaptive mechanism when the error converges to a small threshold value.

A nominal model should be first chosen as an ideal system, then feedback gains  $k_p$  and  $k_v$  are tuned for primary tracking. Using the identification results, the estimated system parameters can be determined. Finally, the control gain  $K_c$  and switch gain  $K_s$  in the sliding mode can be tuned to obtain acceptable transient and steady performance. Details refer to [8].

It can be seen from (46) and (47) that both the two schemes need to obtain a linear model of the system in advance. In the experiments, the linear part of the PEA system is identified through the input–output data excited by a chirp signal between 0.01 to 100 Hz. Using the system identification toolbox in MATLAB, a linear plant is obtained as:

$$\ddot{x} + 195.2\dot{x} + 30515 = 32064u. \quad (48)$$

### 5.1.3. OLNN-SMC

The amount of the neurons adopted in the  $\Phi$  is selected as  $n = 8$ , and the activation functions are chosen as:

$$\begin{cases} \phi_1 = 1/(1 + e^{-0.1x}), & \phi_5 = \phi_1^2, \\ \phi_2 = 1/(1 + e^{-0.2x}), & \phi_6 = \phi_2^2, \\ \phi_3 = 1/(1 + e^{-0.5x}), & \phi_7 = \phi_1 \cdot \phi_2, \\ \phi_4 = 1/(1 + e^{-x}), & \phi_8 = \phi_3 \cdot \phi_4. \end{cases} \quad (49)$$

Note that the activation functions as well as neuron number can be selected according to the user's experience or by a trial and error approach [27,36].

Parameters in the OLNN part is suggested to be determined in the online identification process alone. Detailed steps are: (1) Shut down the feedback SMC mechanism in the whole control scheme; (2) Feed a low-frequency harmonic control signal to drive the system; (3) Use the updating law in (17) to train the NNs; (4) Observe the estimated control signal  $\hat{u} = \hat{\Theta}\Psi$  and compare it with the input control signal  $u$ ; (5) Tune the parameters to minimize the errors between  $\hat{u}$  and  $u$ . Based on the authors' experience, a tradeoff between convergence speed and oscillation should be made by tuning a proper  $\rho$ . It is suggested that  $\rho$  can be initialized as a small value and be increased gradually until the NN approximation errors can be decreased without bring severe oscillation into the system. This criterion is also applicable to the determination of the adaptive gain  $\alpha$ .

After determination of the parameters in the OLNN part, the SMC mechanism can be turned on. The parameter then can be tuned during the experiments to be larger enough gradually in the experiments according to the convergence rate and chattering. It should be noted that the parameters  $k_\sigma$  and  $k_\alpha$  are irrelevant with the stability which can be seen from the proof of **Theorem 2 and 3**, they are set as 0.5 for this case. The value of  $\delta$  is chosen as an acceptable threshold of the tracking error. The filter parameter  $\gamma = 1/(2\pi \cdot 100)$  to reject high-frequency noises.

Other parameters are in **Table 1**. To this end, the determination and tuning of the parameters can be summarized as below. Through simulation cases, the parameters in **Table 1** can be preliminarily initialized. Subsequently, considering that the actual experimental platform suffers from the inevitable uncertainties (i.e., system/parameter perturbation, environmental disturbance, humidity and temperature variations and so on), the parameters are tuned they can be tuned and determined elaborately and carefully by an iterative trial and error method to get the proper anticipated performance for each specified controller in the experiments. This ensures that the comparison of outcomes achieved are suitably fair, as each specified controller has essentially been appropriately and properly tuned.

## 6. Results and discussions

### 6.1. Online identification validation

The online identification is preliminarily conducted through feeding a sinusoidal wave (1 Hz) into the system. Results of the converged weights are shown in **Fig. 4**. It can be intuitively found that the estimated weights all converge in a short period of time. Besides, the estimated  $\hat{c}$  is also close to the identified  $\hat{c}_0 = \hat{m}/\hat{a}$ . The main reason for the gap between  $\hat{c}$  and  $\hat{c}_0$  may be the parameter perturbation of the system. As pointed out in [4,11], variations of external environment (i.e., temperature or vibration) may lead to such parameter perturbation. Herein, this is also the motivation of this work to utilize the online identification method. For this system, the results indicate that the estimation process of the OLNN scheme is stable so that it can be applied in further controller synthesis.

For a scenario of online identification and control for the 1 Hz sinusoidal wave, control input results are shown in **Fig. 5**. It can be seen that the proposed OLNN-SMC can achieve steady online identification results and the control inputs can converge to steady values within 5 periods for this case. Taking a closer look into the components in the control signal, it is found that the feedforward compensator  $u_{nn}$  dominates the whole control input which implies that estimated values of nonlinearities are well compensated by the online NNs. The residual error due to NN approximation and external environment are decreased by the feedback component  $u_{smc}$ . Hence, the tracking performance can be improved by the cooperation of the

**Table 1**  
Parameters of controllers.

Controller	Notation	Value
PID+DOB	$k_p, k_i, k_d, \gamma_1$	0.644, 101, 0, 1/(2 $\pi \cdot 100$ )
ASMC	$m_n, b_n, k_n, K_p, K_v, \hat{m}, \hat{b}, \hat{k}, \hat{a}, \lambda_2, K_c, K_s, \epsilon$	0.001, 1000, 20000, 101, 0.644 1, 195.2, 30515, 32064 300, 0.1, 0.01, 1
OLNN-SMC	$\gamma, \mu, v, \rho, k_\sigma, k_\alpha, \alpha, \delta$	1/(2 $\pi \cdot 100$ ), 0.5, 0.1, 5000, 0.5, 0.5, 0.1, 0.05

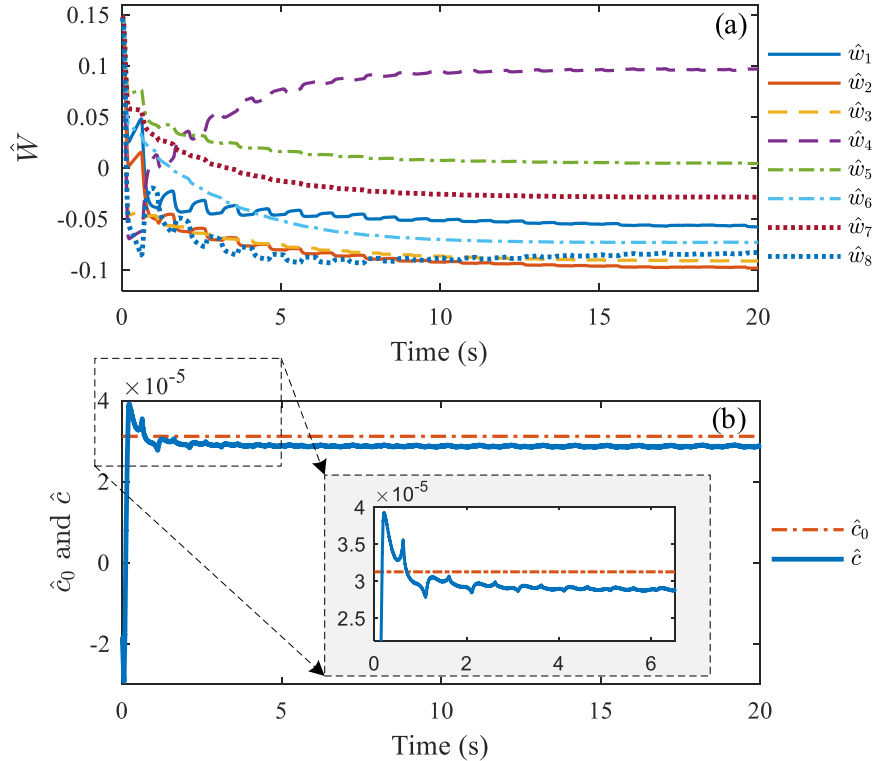


**Fig. 4.** Convergence in the approximation process of the proposed OLNN-SMC. (a) The weights in  $\hat{W}$ . (b) Estimated control gain inversion  $\hat{c}$  using OLNN-SMC and  $\hat{c}_0 = \hat{m}/\hat{a}$ .

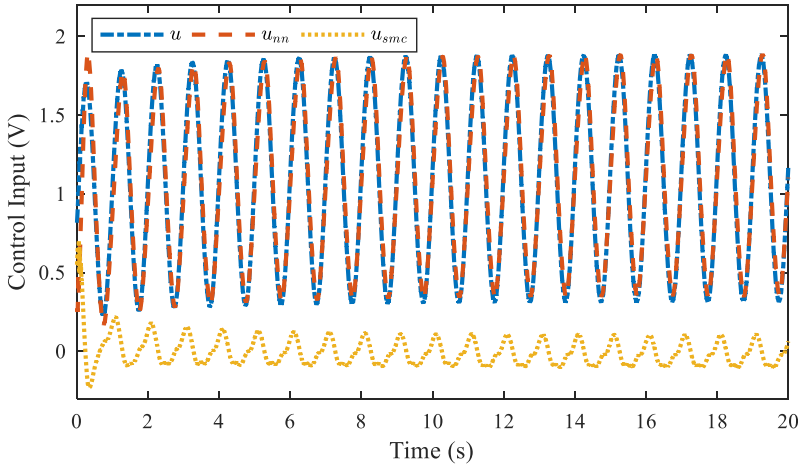


**Fig. 5.** Control inputs of online identification using the proposed OLNN-SMC.

online identification and control in the proposed OLNN-SMC scheme. More tracking cases under different frequencies can be found in the following subsections.

## 6.2. Control scheme validation

As aforementioned, the main goal of the proposed composite control law is to achieve precision motion tracking in the presence of nonlinearities and to maintain robust performance under external disturbances. To validate the effectiveness of the proposed controller, sinusoidal trajectories ranging from 0.1 to 10 Hz are used for the references. The effects of

nonlinearity compensation and tracking precision can be studied both qualitatively and quantificationally through comparisons among open loop (no controller), PID+DOB, ASMC and the proposed OLNN-SMC.

For the convenience of quantificational comparison, some error indexes are defined in advance as:

$$\begin{aligned} e_{RL} &= \max\left(\frac{|x(i)-x_d(i)|}{A}\right) \times 100\%, \\ e_{rms} &= \sqrt{\frac{\sum_{i=1}^N (x(i)-x_d(i))^2}{N}}, \\ e_{max} &= \max(|x(i)-x_d(i)|), \end{aligned} \quad (50)$$

where  $e_{RL}$ ,  $e_{rms}$  and  $e_{max}$  are respectively denoted as the relative error of linearity, the root-mean-square (RMS) error and the maximum tracking error,  $x$  and  $x_d$  are the measured output displacement and the reference trajectory,  $i$  is the discrete index,  $A$  is the stroke of the reference,  $N$  is the length of the data.

### 6.2.1. Results of nonlinearity compensation

Tracking results of sinusoidal trajectories at four frequencies are displayed in Fig. 6. A baseline which starts from the origin point with a slope of 1 is added into the figures to make direct comparisons. For the open loop scenario, obvious hysteresis circles can be observed in all the four tests. In addition, a drift from the baseline is mainly resulted from the creep property. Hence, controllers are required to compensate the nonlinearities. It can be found that all the three controllers alleviate the effects of nonlinearities. In particular, according to the statistical results in Table 2, the relative error of linearity  $e_{RL}$  of the three controllers are maintained under 5% for references within 2 Hz. However, for the 10 Hz case, the  $e_{RL}$  increases dramatically for the controllers except the proposed OLNN-SMC. The reason for PID+DOB case lies in the restricted feedback loop bandwidth, and it tends to be much severer when increasing the PID gains. While for the ASMC case, a nominal model is pre-defined and utilized in the control scheme. It can be easily tracked in low frequencies, but model uncertainties may bring bigger burden to the controller with the increase of frequency.

For the proposed OLNN-SMC scheme, the nonlinearities are well compensated through the feedforward component in the composite control law which is based on the online trained neural networks. The residual online identification error as well as the model uncertainty can be eliminated through the feedback sliding mode component. As a result, the errors of  $e_{RL}$  for these frequencies are all decreased within 5% as listed in Table 2.

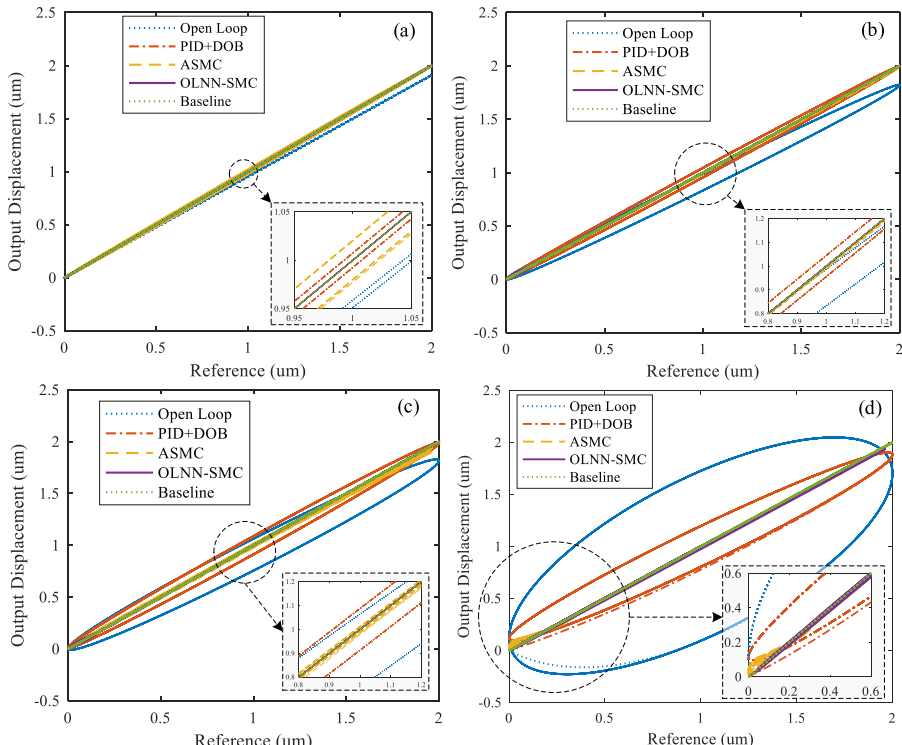


**Fig. 6.** Results of nonlinearity compensation for sinusoidal tracking under the controllers. (a) 0.1 Hz. (b) 1 Hz. (c) 2 Hz. (d) 10 Hz.

**Table 2**

Statistical tracking errors under different controllers.

Errors	Open Loop	PID+DOB	ASMC	OLNN-SMC
$e_{RL}$ (%)	0.1 Hz	4.5121	1.1937	1.5898
	1 Hz	10.4547	2.2484	1.6171
	2 Hz	13.5094	4.4370	3.0169
	10 Hz	47.0483	21.2557	7.4933
$e_{rms}$ ( $\mu m$ )	0.1 Hz	0.0552	0.0026	0.0035
	1 Hz	0.1233	0.0316	0.0091
	2 Hz	0.1560	0.0625	0.0158
	10 Hz	0.6021	0.2842	0.0481
$e_{max}$ ( $\mu m$ )	Hybrid	-	0.4277	0.2687
				0.0678

### 6.2.2. Results of sinusoidal tracking

Overall tracking view and the errors are shown in Fig. 7. It is intuitive that a best tracking performance is achieved by using the proposed OLNN-SMC as the tracking errors are consistently smaller than other cases. Periodic errors which are positively related to the references exist in both the PID+DOB and ASMC cases. As analyzed before, the two schemes can not handle the residual errors under the system perturbation of the entire model or partial parameters. There is also a shortcoming in OLNN-SMC, i.e., the transient oscillation at the beginning of the trajectory. This is a hybrid result from the online NN and SMC, some efforts have been made to alleviate this problem such as chattering-free SMC in [1] and composite learning method for NN in [29]. However, this is not the emphasis of this work. We here conducted online adjustment of the parameters in Table 1 to obtain acceptable transient responses.

To be more specific, the RMS error of 10 Hz tracking under OLNN-SMC is  $0.0074 \mu m$ , which only accounts for 2.6% and 15.4% of that under PID+DOB and ASMC schemes. More detailed data of tracking errors can be found in Table 2.

### 6.2.3. Results of disturbance rejection

To evaluate the robustness of the three controllers, an input disturbance is added when tracking a hybrid reference with 2 and 5 Hz. The amplitudes of both the two components are set as  $2 \mu m$ . The disturbance is set as a step with an amplitude of  $1 \mu m$ , and it occurs at 2.5 s. Results of overall tracking and control inputs of the three controllers are shown in Fig. 8 and Fig. 9.

According to the results in Fig. 8, all the three control scheme can maintain robust stability for the input disturbance. for each control scheme, it takes a short period for the system to recover from transient chattering when the disturbance comes. Taking a closer view into the robust performance, the overall tracking errors of PID+DOB are larger than the other two schemes in both the steady and transient periods. For the ASMC scheme, there are still some periodic steady errors along with the time axis. Besides, the transient chattering is severer than that of OLNN-SMC. Due to the adaptive mechanism in

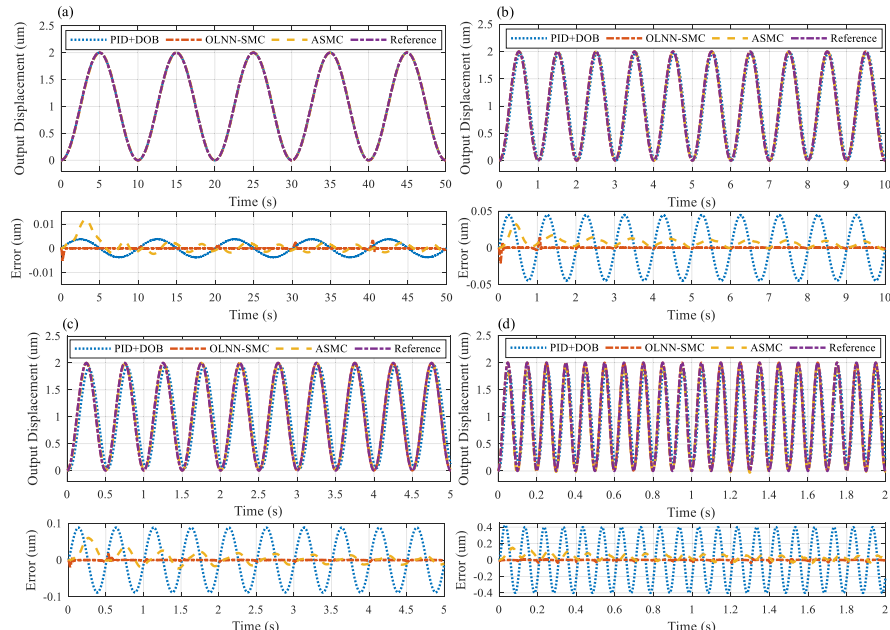


**Fig. 7.** Tracking results of sinusoidal tracking under the controllers. (a) 0.1 Hz. (b) 1 Hz. (c) 2 Hz. (d) 10 Hz.

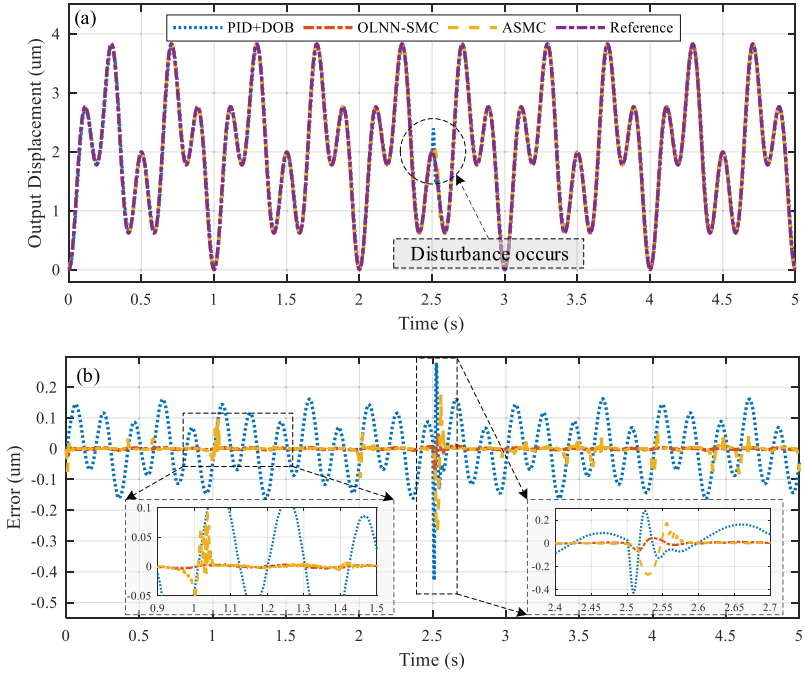


**Fig. 8.** Results of disturbance rejection for hybrid frequency sinusoidal tracking. (a) Overall tracking view. (b) Tracking errors.

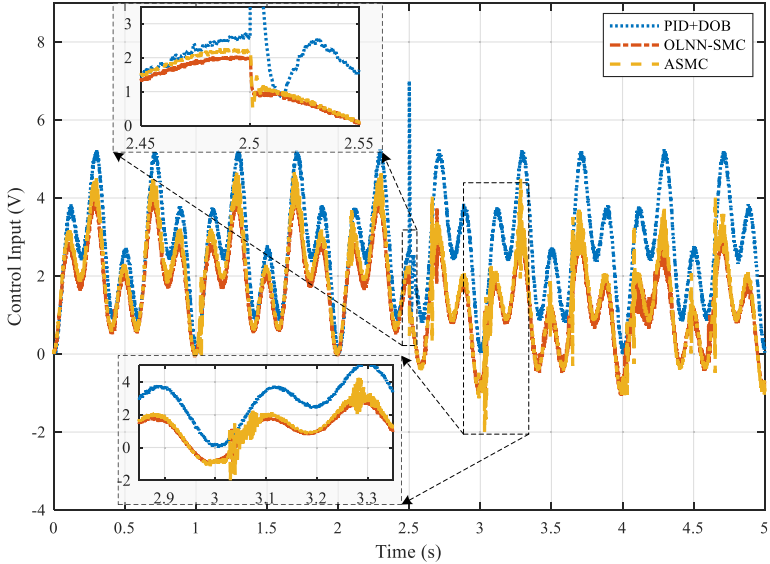


**Fig. 9.** Control inputs of the three controllers for disturbance rejection in hybrid frequency sinusoidal tracking.

the proposed OLNN-SMC scheme, transient chattering is quickly taken out and tracking performance after the transient period recovers subsequently as that before the disturbance occurs.

The control inputs of the three controllers are depicted in Fig. 9. It can be evidently observed that control of PID+DOB consumes more energy than the other two controllers for that the amplitudes of control inputs are larger within the whole time period. In addition, the control perturbation is obvious when the disturbance comes. For some occasions, sudden and large control perturbations will result in damage to physical prototypes. Chattering phenomenon can be alleviated to some extent with the positive effect of the adaptive law in the ASMC and the proposed OLNN-SMC schemes. Hence, compared with PID+DOB, control inputs of the ASMC and the proposed OLNN-SMC are remarkably smoother when rejecting the disturbance. However, due to unmatched system dynamics between the actual system and the identified nominal model in the ASMC

scheme, the generated control input of ASMC is a bit oscillating. This leads to deteriorated tracking performance when compared with the proposed OLNN-SMC scheme. Herein, the results in Fig. 9 demonstrate the proposed OLNN-SMC can reject the disturbance and improve the tracking performance effectively.

Quantitative comparations among the three controllers can be made from Table 2. The maximum transient errors under PID+DOB and ASMC are  $0.4277 \mu\text{m}$  and  $0.2687 \mu\text{m}$ , which are respectively 6.3 and 4.0 times as much as that of  $0.0678 \mu\text{m}$  achieved by OLNN-SMC.

### 6.3. Discussions

The above analysis upon experimental results mainly conducted through comparisons among open loop, PID+DOB, ASMC and the proposed OLNN-SMC. Results of the open loop demonstrated the inherent nonlinearities of the PEA system. All the three controller can alleviate this problem to some extent. For the PID+DOB scheme, restricted bandwidth and exact model are the two main drawbacks, which will lead to failure in high-frequency tracking. For the ASMC scheme, performance is also deteriorated when the model and/or parameter suffers from a perturbation. Although there is an adaptive mechanism in this scheme, perturbations will lead to severe burdens to the controller. The two issues which are also the main problems in most relevant works [8,25,35] can be avoidable by the proposed OLNN-SMC scheme. In addition, unlike the offline trained NN for PEA system in [14,15], the OLNN is more suitable for practical applications without any offline computation, especially in the presence of external disturbance and large uncertainties. Through applying the singularity-free NNs, the OLNN-SMC also has the advantage over [24] in that the convergence process is smoother.

Robustness is an important issue in practical application. Some works have studied enhanced robustness of the control system under multifarious uncertainties or disturbances, such as communication delay [37], partially unknown and uncertain multiagent systems [38] and on-line measuring error [39], etc. Unlike the above works, this paper is mainly dedicated to improvement of robustness versus residual approximation error from the online NN and external disturbance from the environment. Thus, adaptive sliding mode control scheme is more appropriate to merge with the online NN scheme. In the experiments, there are unavoidable modeling errors and disturbances (e.g., sensor noise), and thus the robustness of the proposed control scheme has been tested in the experiments.

To this end, the proposed OLNN-SMC scheme is attractive for applications mainly due to i) nonlinearity model free; ii) singularity free; iii) robustness and adaptive ability to unknown disturbances. To be honest, there is also a shortcoming in the proposed OLNN-SMC, i.e., the transient oscillation at the beginning of the trajectory. This is a hybrid phenomenon resulted from the chattering characteristic of the online NN and SMC. Chattering effect may excite unwanted high-frequency dynamics of the system and reduce the usable life of the actuator [1]. Fortunately, a lot efforts have been made to alleviate this problem such as chattering-free SMC in [1,40–42], composite learning method for NN in [29], and the adaptive neural network control in [34,43]. The proposed OLNN-SMC can be improved further through combing with these chattering-free techniques. However, this is not the emphasis of this work.

## 7. Conclusion

In this paper, a novel online neural-network-based sliding model control scheme is proposed for a class of PEA systems with inherent nonlinearity and external disturbance. A composite control law is synthesized which contains a neural-network-based feedforward component for nonlinearity compensation and an adaptive sliding-mode-based feedback component. Experimental results have verified a better tracking performance of this scheme compared to existing PID+DOB and ASMC. The significance of this work lies in that it not only provides a new online identification and control scheme for PEA systems, but also includes a rigorous theoretical support for precision motion tracking of the scheme under unknown disturbances. The experiments can be easily extended to other PEA platforms such as PEA nanopositioners, PEA surgical devices, PEA microgrippers, etc. It is worth noting that the chattering property in current design can be alleviated using other sliding mode functions. In addition, the tracking accuracy can be further improved by reducing the residual errors of the online identification in Theorem 1. These are interesting topics for further studies.

### CRediT authorship contribution statement

**Jie Ling:** Methodology, Validation, Data curation, Writing - original draft. **Zhao Feng:** Conceptualization, Writing - review & editing. **Dongdong Zheng:** Conceptualization, Writing - review & editing. **Jun Yang:** Writing - review & editing. **Haoyong Yu:** Conceptualization, Writing - review & editing. **Xiaohui Xiao:** Conceptualization, Funding acquisition.

### Declaration of Competing Interest

The authors declare that they have no known competing financial interests or personal relationships that could have appeared to influence the work reported in this paper.

## Acknowledgements

This work was supported by China Postdoctoral Science Foundation [Grant No. 2018M642905], Natural Science Foundation of China [Grant No. 51375349], and Science and Technology Planning Project of Shenzhen Municipality [Grant No. JCYJ20170306171514468].

## References

- [1] Q. Xu, Precision motion control of piezoelectric nanopositioning stage with chattering-free adaptive sliding mode control, *IEEE Transactions on Automation Science and Engineering* 14 (1) (2016) 238–248.
- [2] D. Sabarianand, P. Karthikeyan, T. Muthuramalingam, A review on control strategies for compensation of hysteresis and creep on piezoelectric actuators based micro systems, *Mechanical Systems and Signal Processing* 140 (2020) 106634.
- [3] W. Liang, J. Ma, C. Ng, Q. Ren, S. Huang, K.K. Tan, Optimal and intelligent motion control scheme for an ultrasonic-motor-driven xy stage, *Mechatronics* 59 (2019) 127–139.
- [4] J. Ling, M. Rakotondrabe, Z. Feng, M. Ming, X. Xiao, A robust resonant controller for high-speed scanning of nanopositioners: design and implementation, *IEEE Transactions on Control Systems Technology* 28 (3) (2020) 1116–1123.
- [5] G. Gu, L. Zhu, C. Su, H. Ding, S. Fatikow, Modeling and control of piezo-actuated nanopositioning stages: a survey, *IEEE Transactions on Automation Science and Engineering* 13 (1) (2014) 313–332.
- [6] Y. Zhang, Y. Peng, Z. Sun, H. Yu, A novel stick-slip piezoelectric actuator based on a triangular compliant driving mechanism, *IEEE Transactions on Industrial Electronics* 66 (7) (2018) 5374–5382.
- [7] D. Habineza, M. Zouari, Y. Le Gorrec, M. Rakotondrabe, Multivariable compensation of hysteresis, creep, badly damped vibration, and cross couplings in multiaxes piezoelectric actuators, *IEEE Transactions on Automation Science and Engineering* 15 (4) (2017) 1639–1653.
- [8] J.Y. Lau, W. Liang, K.K. Tan, Adaptive sliding mode enhanced disturbance observer-based control of surgical device, *ISA Transactions* 90 (2019) 178–188.
- [9] M.S. Rana, H.R. Pota, I.R. Petersen, A survey of methods used to control piezoelectric tube scanners in high-speed afm imaging, *Asian Journal of Control* 20 (4) (2018) 1379–1399.
- [10] J. Gan, X. Zhang, A review of nonlinear hysteresis modeling and control of piezoelectric actuators, *AIP Advances* 9 (4) (2019) 040702.
- [11] M. Rakotondrabe, Multivariable classical prandtl-ishlinskii hysteresis modeling and compensation and sensorless control of a nonlinear 2-dof piezoactuator, *Nonlinear Dynamics* 89 (1) (2017) 481–499.
- [12] L. Fang, J. Wang, Q. Zhang, Identification of extended hammerstein systems with hysteresis-type input nonlinearities described by Preisach model, *Nonlinear Dynamics* 79 (2) (2015) 1257–1273.
- [13] M. Al Janaihah, M. Al Saideh, M. Rakotondrabe, On hysteresis modeling of a piezoelectric precise positioning system under variable temperature, *Mechanical Systems and Signal Processing* 145 (2020) 106880.
- [14] L. Cheng, W. Liu, Z. Hou, J. Yu, M. Tan, Neural-network-based nonlinear model predictive control for piezoelectric actuators, *IEEE Transactions on Industrial Electronics* 62 (12) (2015) 7717–7727.
- [15] W. Liu, L. Cheng, Z. Hou, J. Yu, M. Tan, An inversion-free predictive controller for piezoelectric actuators based on a dynamic linearized neural network model, *IEEE/ASME Transactions on Mechatronics* 21 (1) (2015) 214–226.
- [16] S. Salapaka, A. Sebastian, J.P. Cleveland, M.V. Salapaka, High bandwidth nano-positioner: a robust control approach, *Review of Scientific Instruments* 73 (9) (2002) 3232–3241.
- [17] B.E. Heflrich, C. Lee, D.A. Bristow, X. Xiao, J. Dong, A.G. Alleyne, S.M. Salapaka, P.M. Ferreira, Combined  $h_\infty$ -feedback control and iterative learning control design with application to nanopositioning systems, *IEEE Transactions on Control Systems Technology* 18 (2) (2009) 336–351.
- [18] J.Y. Peng, X.B. Chen, Integrated pid-based sliding mode state estimation and control for piezoelectric actuators, *IEEE/ASME Transactions on Mechatronics* 19 (1) (2012) 88–99.
- [19] J.P. Mishra, Q. Xu, X. Yu, M. Jalili, Precision position tracking for piezoelectric-driven motion system using continuous third-order sliding mode control, *IEEE/ASME Transactions on Mechatronics* 23 (4) (2018) 1521–1531.
- [20] S. Huang, K.K. Tan, T.H. Lee, Adaptive sliding-mode control of piezoelectric actuators, *IEEE Transactions on Industrial Electronics* 56 (9) (2009) 3514–3522.
- [21] Y. Zhang, P. Yan, Adaptive observer-based integral sliding mode control of a piezoelectric nano-manipulator, *IET Control Theory & Applications* 13 (14) (2019) 2173–2180.
- [22] F.J. Lin, H.J. Sheih, P.K. Huang, Adaptive wavelet neural network control with hysteresis estimation for piezo-positioning mechanism, *IEEE Transactions on Neural Networks* 17 (2) (2006) 432–444.
- [23] F.J. Lin, H.J. Sheih, P.K. Huang, L.T. Teng, Adaptive control with hysteresis estimation and compensation using rfn for piezo-actuator, *IEEE Transactions on Ultrasonics, Ferroelectrics, and Frequency Control* 53 (9) (2006) 1649–1661.
- [24] J.Y. Lau, W. Liang, K.K. Tan, Motion control for piezoelectric-actuator-based surgical device using neural network and extended state observer, *IEEE Transactions on Industrial Electronics* 67 (1) (2019) 402–412.
- [25] W.H. Chen, J. Yang, L. Guo, S. Li, Disturbance-observer-based control and related methods – an overview, *IEEE Transactions on Industrial Electronics* 63 (2) (2015) 1083–1095.
- [26] D. Zheng, W. Xie, T. Chai, Z. Fu, Identification and trajectory tracking control of nonlinear singularly perturbed systems, *IEEE Transactions on Industrial Electronics* 64 (5) (2016) 3737–3747.
- [27] D. Zheng, Y. Pan, K. Guo, H. Yu, Identification and control of nonlinear systems using neural networks: a singularity-free approach, *IEEE Transactions on Neural Networks and Learning Systems* 30 (9) (2019) 2696–2706.
- [28] F. Lewis, S. Jagannathan, A. Yesildirkak, *Neural Network Control of Robot Manipulators and Non-linear Systems*, CRC Press, 1998.
- [29] Y. Pan, T. Sun, Y. Liu, H. Yu, Composite learning from adaptive backstepping neural network control, *Neural Networks* 95 (2017) 134–142.
- [30] J. Na, S. Wang, Y. Liu, Y. Huang, X. Ren, Finite-time convergence adaptive neural network control for nonlinear servo systems, *IEEE Transactions on Cybernetics* 50 (6) (2020) 2568–2579.
- [31] H.K. Khalil, J.W. Grizzle, *Nonlinear Systems*, vol. 3, Prentice hall, Upper Saddle River, NJ, 2002.
- [32] B. Li, X. Rui, Vibration control of uncertain multiple launch rocket system using radial basis function neural network, *Mechanical Systems and Signal Processing* 98 (2018) 702–721.
- [33] H. Taghavifar, S. Rakheja, Path-tracking of autonomous vehicles using a novel adaptive robust exponential-like-sliding-mode fuzzy type-2 neural network controller, *Mechanical Systems and Signal Processing* 130 (2019) 41–55.
- [34] J. Na, X. Ren, D. Zheng, Adaptive control for nonlinear pure-feedback systems with high-order sliding mode observer, *IEEE Transactions on Neural Networks and Learning Systems* 24 (3) (2013) 370–382.
- [35] J. Yi, S. Chang, Y. Shen, Disturbance-observer-based hysteresis compensation for piezoelectric actuators, *IEEE/ASME Transactions on Mechatronics* 14 (4) (2009) 456–464.
- [36] M. Chen, S.S. Ge, Adaptive neural output feedback control of uncertain nonlinear systems with unknown hysteresis using disturbance observer, *IEEE Transactions on Industrial Electronics* 62 (12) (2015) 7706–7716.

- [37] D. Zhang, Z. Xu, G. Feng, H. Li, Asynchronous resilient output consensus of switched heterogeneous linear multivehicle systems with communication delay, *IEEE/ASME Transactions on Mechatronics* 24 (6) (2019) 2627–2640.
- [38] Z. Xu, H. Ni, H. Reza Karimi, D. Zhang, A markovian jump system approach to consensus of heterogeneous multiagent systems with partially unknown and uncertain attack strategies, *International Journal of Robust and Nonlinear Control* 30 (7) (2020) 3039–3053.
- [39] H. Zhang, J. Wang, Active steering actuator fault detection for an automatically-steered electric ground vehicle, *IEEE Transactions on Vehicular Technology* 66 (5) (2016) 3685–3702.
- [40] S. Wang, L. Tao, Q. Chen, J. Na, X. Ren, Usde-based sliding mode control for servo mechanisms with unknown system dynamics, *IEEE/ASME Transactions on Mechatronics* 25 (2) (2020) 1056–1066.
- [41] Z. Feng, W. Liang, J. Ling, X. Xiao, K.K. Tan, T.H. Lee, Integral terminal sliding-mode-based adaptive integral backstepping control for precision motion of a piezoelectric ultrasonic motor, *Mechanical Systems and Signal Processing* 144 (2020) 106856.
- [42] R.M. Asl, Y.S. Hagh, S. Anavatti, H. Handroos, Adaptive finite integral non-singular terminal synergetic control of nth-order nonlinear systems, *Mechanical Systems and Signal Processing* 142 (2020) 106789.
- [43] J. Na, J. Yang, G. Gao, Reinforcing transient response of adaptive control systems using modified command and reference model, *IEEE Transactions on Aerospace and Electronic Systems* 56 (3) (2020) 2005–2017.